Neuron, Vol. 33, 921–933, March 14, 2002, Copyright ©2002 by Cell Press

Distinct NMDA Receptors Provide Differential Modes of Transmission at Mossy Fiber-Interneuron Synapses

Saobo Lei and Chris J. McBain[1]
[1]Laboratory of Cellular and Molecular Neurophysiology
National Institute of Child Health and Human Development
National Institutes of Health
49 Convent Drive
Bethesda, Maryland 20892

Summary

Dentate gyrus granule cells innervate inhibitory interneurons via a continuum of synapses comprised of either Ca^{2+}-impermeable (CI) or Ca^{2+}-permeable (CP) AMPA receptors. Synapses at the extreme ends of this continuum engage distinct postsynaptic responses, with activity at CI synapses being strongly influenced by NMDA receptor activation. NMDARs at CI synapses have a lower NR2B subunit composition and a higher open probability, which generate larger amplitude and more rapid EPSCs than their CP counterparts. A novel form of NMDAR-dependent long-term depression (iLTD) is associated with CI-mossy fiber synapses, whereas iLTD at CP synapses is dependent on Ca^{2+}-permeable AMPA receptor activation. Induction of both forms of iLTD required elevation of postsynaptic calcium. Thus mossy fibers engage CA3 interneurons via multiple synapse types that will act to expand the computational repertoire of the mossy fiber-CA3 network.

Introduction

Within the CA3 hippocampus, the axons of dentate gyrus granule cells, the so-called mossy fibers, innervate pyramidal cells via large, complex mossy boutons, while inhibitory interneurons of the CA3 stratum lucidum are preferentially targeted by either small en passant or filopodial mossy fiber terminals (Acsady et al., 1998). This anatomical segregation is accompanied by a functional specialization of mossy fiber transmission that depends on the nature of the postsynaptic target (Maccaferri et al., 1998; Toth and McBain, 1998; Toth et al., 2000). At mossy fiber-principal neuron synapses, AMPA receptors comprise a high level of GluR2 expression, which renders these receptors essentially Ca^{2+} impermeable (Spruston et al., 1995; Toth et al., 2000). In contrast, hippocampal interneurons express heterogeneous levels of GluR2 (Leranth et al., 1996; He et al., 1998) and mossy fiber-interneuron synapses are comprised of either Ca^{2+}-impermeable or Ca^{2+}-permeable AMPARs (referred to as "CI" and "CP" synapses, respectively hereafter) (Toth et al., 2000; McBain and Fisahn, 2001). Moreover, both synapse types can exist on single interneurons (Toth and McBain, 1998). Consequently, the properties of AMPA receptor-mediated mossy fiber-interneuron transmission depends on the nature of the synapse being activated (Toth and McBain, 1998; Toth et al., 2000). Furthermore, paradigms that induce an NMDA-independent form of long-term potentiation (LTP) at mossy fiber-principal synapses induce a NMDAR-independent form of long-term depression at CP-interneuron synapses, while no long-term synaptic plasticity has been described at CI synapses.

Mossy fiber-pyramidal neuron synapses differ from most central synapses in that they are generally considered to contain few NMDA receptors (Monaghan and Cotman, 1985; Jonas et al., 1993; Siegel et al., 1994; Watanabe et al., 1998; Weisskopf and Nicoll, 1995). The ratio of NMDA receptor-mediated to AMPA receptor-mediated EPSCs at mossy fiber-principal neuron synapses is ~30% of that found at CA3 associational-commissural-principal cell synapses (Weisskopf and Nicoll, 1995). Moreover, one of the hallmark features of the mossy fiber-principal cell synapse is its apparent lack of NMDAR-dependent synaptic plasticity and suggests that induction of mossy fiber LTP may be nonassociative, noncooperative, and non-Hebbian (Chattarji et al., 1989; Langdon et al., 1995; Zalutsky and Nicoll, 1992). While the nature and function of AMPARs at mossy fiber-interneuron synapses are well described, no confirmation of NMDA receptors at either synapse type exists. Moreover, the potential for differential distribution and properties of NMDARs at synapses containing Ca^{2+}-permeable- or Ca^{2+}-impermeable AMPARs is completely unexplored. Of particular importance, the colocalization of NMDARs and Ca^{2+}-permeable AMPARs at single hippocampal interneuron synapses could potentially provide multiple routes for Ca^{2+} entry, which are likely to be important for synaptic transmission, plasticity, or excitotoxicity.

Here we demonstrate that mossy fiber-interneuron synapses represent a continuum of synapse types, ranging from synapses comprising CP-AMPA receptors to CI-AMPA receptors. At the two extremes of this continuum, NMDARs differ in their kinetics, subunit composition, and open probability. These properties allow mossy fibers to engage their interneuron targets with distinct physiological and long-term-plastic properties.

Results

Large Amplitude NMDA EPSCs Are Preferentially Expressed at CI Synapses

Mossy fibers innervate CA3 stratum lucidum interneuron targets via synapses comprised of philanthotoxin (PhTx)-sensitive, calcium-permeable AMPARs, or PhTx-insensitive, calcium-impermeable AMPARs (Toth and McBain, 1998; Toth et al., 2000). The presence or absence of NMDARs at either synapse type, however, has not been established. First we isolated the NMDAR and AMPAR EPSCs at mossy fiber synapses using an experimental protocol that allowed us to identify both the Ca^{2+}-permeable nature of the AMPARs as well as determine NMDAR properties at individual synapses. Figure 1A

[1]Correspondence: chrismcb@codon.nih.gov

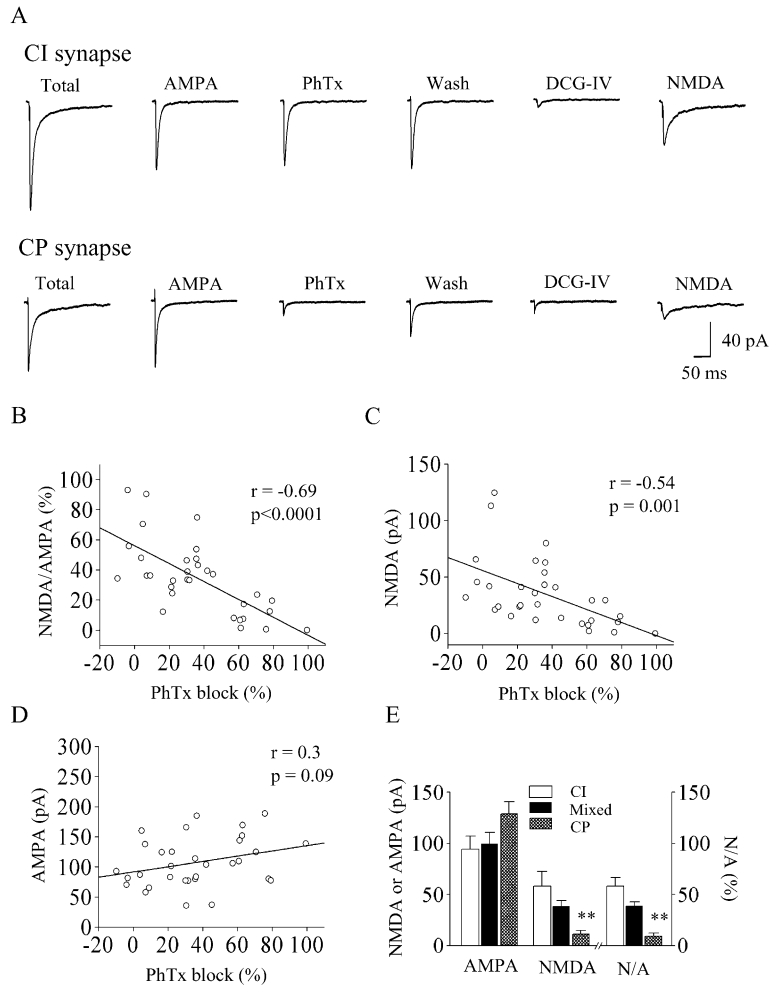

Figure 1. Small Amplitude NMDA Receptor-Mediated EPSCs Are Associated with CP Synapses

(A) EPSCs recorded from a CI (upper panel) and a CP (lower panel) synapse under conditions used to isolate either AMPAR- or NMDAR-mediated components. Total EPSCs comprising both NMDA and AMPA receptor-mediated components were initially recorded in an extracellular solution containing no added Mg^{2+} at a holding potential of −60 mV. AMPA EPSCs were isolated by subsequent application of Mg^{2+} (1.5 mM) and APV (100 μM). The Ca^{2+}-permeable nature of AMPA receptor EPSCs was then assessed by perfusing the slice with philanthotoxin (PhTx, 5 μM), which blocks currents through Ca^{2+}-permeable AMPA receptors (lower panel) but preserves currents through Ca^{2+}-impermeable AMPA receptors (upper panel). DCG-IV (1 μM) was then added to confirm that synaptic responses were mediated by stimulation of mossy fiber axons. Traces in each panel of this figure were average currents from 50 to 100 EPSCs. The NMDA component (right) was obtained by subtracting the averaged AMPA EPSC from the total EPSC.

(B–D) Plots of the percentage of philanthotoxin block versus the ratio of NMDAR:AMPAR EPSC amplitudes (B), NMDA EPSC amplitudes (C), and AMPA EPSC amplitudes (D) reveal a negative correlation between the NMDAR EPSC amplitude and PhTx block.

(E) Summary of the data from 8 CI synapses, 10 CP synapses, and 14 synapses that possessed intermediated PhTx sensitivity (Mixed). **, $p < 0.01$.

shows the results from a typical experiment. The total EPSC mediated by both NMDA and AMPARs was initially recorded in an extracellular solution containing no added Mg^{2+}. The AMPAR component was then isolated by perfusion with a solution containing Mg^{2+} (1.5 mM) and *dl*-APV (100 μM). Subsequent application of PhTx (5 μM), a high-affinity antagonist of currents through calcium-permeable AMPAR channels (Blaschke et al., 1993; Herlitze et al., 1993; Washburn and Dingledine, 1996; Toth and McBain, 1998; Toth et al., 2000), had either little (upper panel, Figure 1A), or significant (lower panel, Figure 1A) inhibitory effect, demonstrating that AMPAR EPSCs comprised Ca^{2+}-impermeable- or Ca^{2+}-permeable AMPARs, respectively (Toth and McBain, 1998). After washing out PhTx, application of the selective group II metabotropic glutamate receptor agonist, DCG-IV (1 μM), inhibited the responses of both synapses confirming that EPSCs were mediated by stimulation of mossy fiber axons (Kamiya et al., 1996; Toth and McBain, 1998; Toth et al., 2000). Subtraction of the AMPA EPSC from the total EPSC waveform yielded the NMDAR EPSC.

Using this protocol, a total of 32 evoked synaptic currents were initially studied. The extent of PhTx inhibition varied significantly between synapses indicating a heterogeneous level of GluR2 expression (Leranth et al., 1996; He et al., 1998). These data suggest that mossy fiber-interneuron synapses comprise a continuum ranging from Ca^{2+}-permeable to Ca^{2+}-impermeable AMPAR-containing synapses (Figures 1B–1D). A plot of the percentage of PhTx block of AMPA EPSCs versus the ratio of NMDA and AMPA EPSC amplitudes showed a negative linear correlation (Figure 1B), demonstrating that the ratio of NMDA and AMPA EPSCs is lowest at the most CP synapses. While no correlation between the amplitudes of AMPA EPSCs and the percentage of PhTx block was observed (Figure 1D), the amplitudes of NMDA EPSCs were negatively correlated with the degree of PhTx block of the AMPA EPSCs (Figure 1C), demonstrating that CP synapses possess smaller amplitude NMDA EPSCs.

Although the above data clearly demonstrates that mossy fiber-interneuron synapses are formed from a continuum of AMPA receptor subtypes, for the purpose of quantitative analysis, throughout the study we have defined AMPAR EPSCs demonstrating >50% block by PhTx as being generated by CP synapses (mean PhTx block, 70.8% ± 4.0%, n = 10) and those displaying <10% block by PhTx as being generated by CI synapses (mean PhTx block, 1.9% ± 2.4%, n = 8) (Washburn and Dingledine, 1996; Toth and McBain, 1998; Toth et al., 2000). Synapses demonstrating PhTx

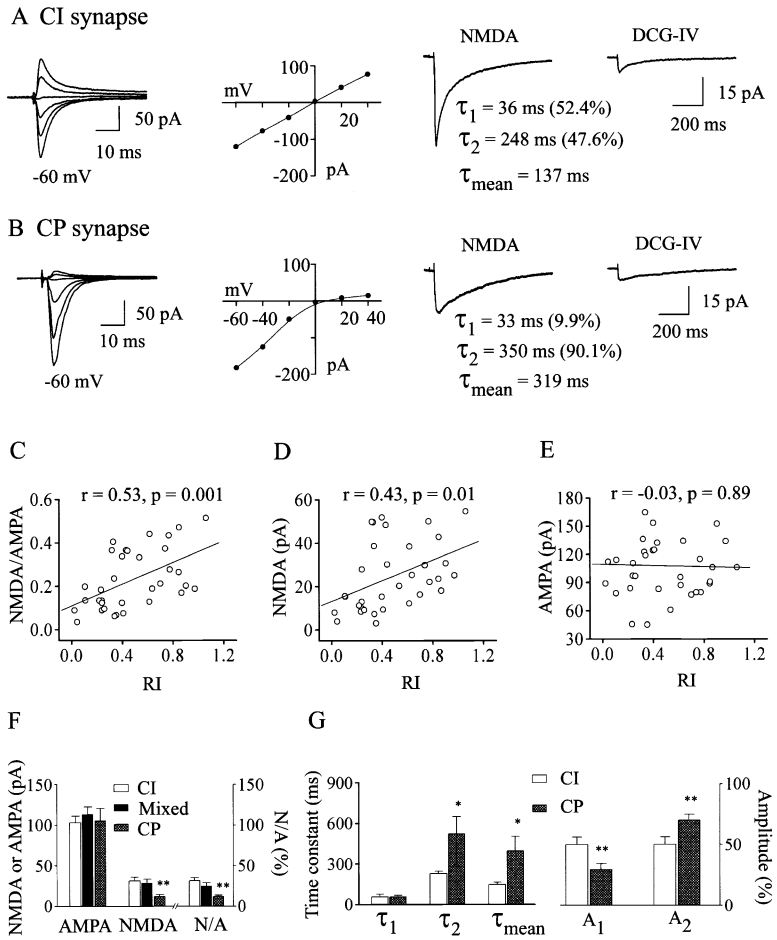

Figure 2. Prolonged Decay Kinetics of NMDA EPSCs at CP Synapses

(A) Current-voltage relationship (I-V) of AMPA EPSCs (two left panels) and the corresponding NMDA EPSC at −60 mV (second from right) at a CI synapse. The linear I-V relationship (RI = 0.97) indicated that this synapse comprised Ca^{2+}-impermeable AMPA receptors. The decay phase of the averaged NMDA EPSC was fit by two exponential functions. Application of DCG-IV (far right) inhibited the NMDA EPSCs, confirming that responses were mediated by mossy fiber stimulation.

(B) I-V relationship of AMPA EPSCs and the corresponding NMDA EPSC at a CP synapse. The strong inward rectification of the I-V relationship (RI = 0.1) indicated that this synapse comprised Ca^{2+}-permeable AMPA receptors. The averaged NMDA EPSC at this synapse had a slower decay time constant.

(C–E) Plots of RI versus the ratio of NMDA:AMPA EPSC amplitudes (C), NMDA EPSC amplitude (D), and AMPA EPSC amplitude (E) from 34 neurons. Note that a correlation exists only between the RI and the NMDA EPSC amplitude and not with the AMPA EPSC amplitude.

(F) Summary of the data from 10 CI, 10 CP, and 14 mixed synapses.

(G) Decay time constants and their relative amplitudes of NMDA EPSCs at CI and CP synapses. **, $p < 0.01$; *, $p < 0.05$.

block between 10%–50% (mean PhTx block, 31.1% ± 2.2%, n = 14), are presumably comprised of AMPA receptors with intermediate Ca permeability or by overlapping populations of CI- and CP-AMPARs. Throughout the manuscript, these are referred to as "mixed" synapses. Figure 1E demonstrates that while AMPA EPSCs amplitude was not significantly different at either CI or CP synapses, CP synapses typically possess significantly smaller NMDAR EPSC amplitudes.

In addition to extracellular polyamine block, GluR2-lacking, Ca^{2+}-permeable AMPARs display inwardly rectifying current-voltage (I-V) relationships in the presence of intracellular polyamines, whereas Ca^{2+}-impermeable AMPARs show nearly linear I-V relationships (Bowie and Mayer, 1995; Koh et al., 1995; Kamboj et al., 1995; Donevan and Rogawski, 1995; Toth and McBain, 1998; Liu and Cull-Candy, 2000). To determine whether a similar relationship existed between NMDA EPSCs and the extent of inward rectification of AMPA EPSCs at mossy fiber-interneuron synapses, we next determined the I-V relationship of AMPAR EPSCs in the presence of APV (100 μM). APV was then washed out and DNQX (10 μM) washed in to isolate the NMDAR EPSC.

Isolated NMDA EPSC's amplitudes at CI synapses (Figure 2A) had larger amplitudes and faster decay kinetics than NMDA EPSCs at CP synapses (Figures 2B and 2G). Plots of the rectification index (RI) versus the ratio of NMDA:AMPA EPSCs, NMDA- and AMPA-EPSC amplitude were constructed from 34 neurons (Figures 2C–2E). Although the RI and the ratio of NMDA:AMPA EPSCs were linearly correlated (Figure 2C), only isolated NMDA EPSC amplitudes were correlated with RI (Figures 2D and 2E). For quantitative analysis, we defined EPSCs possessing a RI > 0.7 as CI synapses (mean RI = 0.85 ± 0.03, n = 10) and those displaying a RI < 0.3 as CP synapses (mean RI = 0.17 ± 0.03, n = 10). Those synapses with RI values between 0.3 and 0.7 (mean RI = 0.44 ± 0.03, n = 14) likely contain varied amounts of GluR2, i.e., were "mixed" synapses. Furthermore, while AMPA EPSC amplitudes were not significantly different across synapse types, NMDA EPSCs and the ratio of NMDA and AMPA EPSCs were larger at CI synapses (Figure 2F).

NMDARs at CP Synapses Have Slower Decay Kinetics

The decay of NMDA EPSCs was best fit by the sum of two-exponential functions. While the first component of the NMDA EPSCs (τ_1) was not significantly different between CI synapses (mean $\tau 1$ = 58.2 ± 19.1 ms, n = 10) and CP synapse (mean $\tau 1$ = 60.8 ± 8.4 ms, n = 10, $p > 0.05$), its relative proportion (A_1) was larger at CI synapses (49.9% ± 6.2% of total amplitude versus 29.8% ± 4.5% at CP synapses, $p < 0.01$) (Figure 2G). The second component (τ_2) was slower (525.9 ± 123.6 versus 228.5 ± 18.1 ms) and its contribution (A_2) larger

at CP synapses (70.2% ± 4.5% versus 50.1% ± 6.2%) (Figure 2G). Therefore, the weighted time constant of NMDA EPSCs (τ_{mean}) at CP synapses was significantly longer than that at CI synapses (Figure 2G). Taken together, these results demonstrate that the NMDA EPSCs at CP synapses are of smaller amplitude and possess slower kinetics than their CI counterparts.

A High NR2B Content of NMDARs at CP Synapses

Native NMDARs are formed by the heteromeric expression of NR1 with one or more NR2 (NR2A–NR2D) subunits (McBain and Mayer, 1994; Dingledine et al., 1999). NR2 subunits determine many of the unique properties of NMDARs including gating kinetics, unitary conductance, ligand binding affinity, kinetics of desensitization and deactivation, and the sensitivity to many channel modulators. Furthermore, NMDAR EPSCs are briefer at synapses containing more NR2A than NR2B subunits (Flint et al., 1997; Stocca and Vicini, 1998; Cathala et al., 2000). To determine whether the slower kinetics of NMDA EPSCs at CP synapses resulted from differences in NR2 subunit expression, we used a specific inhibitor of NR2B-containing NMDARs, ifenprodil (Williams, 1993). Ifenprodil (10 μM) blocked the mean NMDA EPSC amplitude by 41.9% ± 1.9% (n = 10) and 58.6% ± 1.6% (n = 9) at CI and CP synapses, respectively (Figures 3A–3C). While the total NMDA EPSC amplitude was larger at CI synapses (Figure 3C), the relative proportion of ifenprodil-sensitive current (NR2B mediated) was significantly higher at CP synapses (Figure 3D). These results demonstrate that a larger proportion of NR2B subunits contribute to the NMDA receptor EPSCs at CP synapses, consistent with the slower kinetics of NMDA receptor EPSC at these synapses.

Developmental Regulation of CI and CP Synapses

So far we have shown that CP synapses contain AMPARs with a lower GluR2 level and NMDARs with a higher NR2B composition than CI synapses. Within many CNS regions, NR2B and GluR2 expression is developmentally regulated; with high NR2B and low GluR2 being observed at early developmental stages (Monyer et al., 1994; Stocca and Vicini, 1998; Cathala et al., 2000; Pickard et al., 2000; Zhu et al., 2000). We next considered whether CP synapses represented a developmentally immature mossy fiber-interneuron synapse. Using the degree of PhTx block of AMPAR EPSCs as an indicator of CI and CP synapses, we examined synapses from four age groups that spanned developmental stages at which mossy fiber-interneuron synapses appear (Postnatal day [P] 9–10), mature (P15–P16), and then fully develop (P20–P21 and P30–P40) (Amaral and Dent, 1981). At P9–P10, CP synapses were the most predominant synapse type observed (61.3%, 19 of 31), while CI synapses predominated at P30–P40 (45.6%, 14 of 31) (Figure 3E). The intermediate age group of P15–P16 contained the highest percentage of synapses comprised of "mixed" AMPARs, suggesting that this may represent a period of transition from CP to CI synapses (Figure 3E). This was more clearly demonstrated by plotting the percentage of PhTx block for all synapses recorded at all developmental stages (Figure 3F). Although these results indicate that both CI and CP synapses are developmentally regulated, it is worthwhile noting that both synapse types are observed in considerable numbers at all developmental stages.

NMDARs at Both Synapse Types Have Similar Unitary Conductances

We next tested whether the small amplitude of NMDA EPSCs at CP synapses resulted from receptors with a smaller unitary conductance using peak-scaled nonstationary variance analysis to measure the conductance of synaptic NMDARs (Robinson et al., 1991; Traynelis et al., 1993; Traynelis and Jaramillo, 1998; Benke et al., 1998). The single-channel conductances underlying NMDAR EPSCs were not significantly different between the two synapse types (CI synapses, RI = 0.99 ± 0.07, γ_{NMDA} = 46 ± 3 pS, n = 8; CP synapses, RI = 0.19 ± 0.02, γ_{NMDA} = 47 ± 6 pS, n = 7, $p > 0.05$) (Figure 4). These results suggest that differences in single-channel conductance are unlikely to account for the distinct amplitudes of NMDAR EPSCs observed at these two types of synapses.

NMDARs at CP Synapses Have a Lower Open Probability

The open probability of NMDARs at CI and CP synapses was assessed using MK-801, an irreversible open channel blocker (on a time scale of tens of minutes at hyperpolarized potentials) (Huettner and Bean, 1988; Jahr, 1992). In the continued presence of MK-801, NMDAR EPSCs become progressively reduced in amplitude. The rate of block of synaptic NMDA currents by MK-801 is related either to a reduction in presynaptic release probability of glutamate (Hessler et al., 1993; Rosenmund et al., 1993) or to the postsynaptic open probability of NMDA receptors. We have previously shown that short-term plasticity, a phenomenon largely presynaptic in origin, was not different between CI and CP synapses (Toth et al., 2000), suggesting that the release probabilities of glutamate at those two synapse types are similar. We therefore reasoned that any differences in the rate of MK-801 block between these two synapses likely results from a postsynaptic mechanism, i.e., distinct open probabilities of NMDARs at these two types of synapses. Figures 5A and 5B show the time course of MK-801 block of NMDA EPSCs at a CI synapse (RI = 1.16) and a CP synapse (RI = 0.17), respectively. The rate of MK-801 block of the isolated NMDAR EPSC was fit by a double-exponential function, giving rise to a mean time constant of 28.8 stimuli for the CI synapse and 66.9 stimuli for the CP synapse. Figures 5C and 5D show that the mean decay rate was significantly slower at CP synapses.

To ensure that the different rates of MK-801 block observed at CI and CP synapses did not originate from differences in release probability between these two synapses, we compared the paired pulse ratios (PPRs) of AMPA EPSCs at these two types of synapses. PPRs were not significantly different between CI (1.59 ± 0.07, n = 9) and CP synapses (1.64 ± 0.08, n = 9, $p > 0.05$) (Figure 5E). Second, the coefficient of variance (CV = SD/mean), an index also considered to reflect presynaptic processes, was not significantly different between synapse types (CI synapses, 0.23 ± 0.02, n = 9; CP

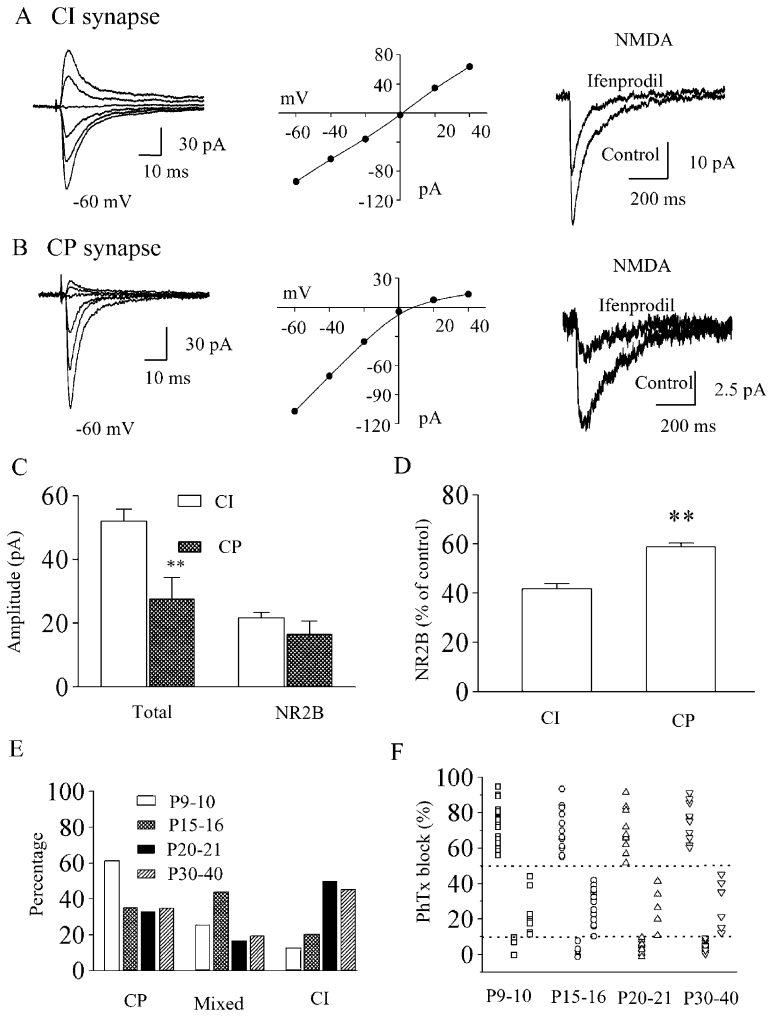

Figure 3. Differences in Subunit Composition and Developmental Regulation of CI and CP Synapses

(A and B) I-V relationship of AMPA EPSC (left two panels) and the isolated NMDA EPSC component associated with this synapse recorded in the absence or presence of the NR2B antagonist, ifenprodil, from a CI (A) and a CP (B) synapse; Ifenprodil blocked NMDA EPSCs by 39% and 61% respectively.

(C and D) Summarized data from ten CI (RI = 0.84 ± 0.05) and nine CP synapses (RI = 0.22 ± 0.03) show that the NR2B content of NMDARs at CP synapses is significantly higher than that at CI synapses. **, $p < 0.01$.

(E and F) Developmental regulation of CI and CP synapses. The sensitivity to PhTx block was used to evaluate the Ca^{2+}-permeable nature of AMPARs at each synapse. For each age group, at least 30 synapses were examined (individual symbols in F) and the incidence of each synapse type determined. The percentage of CP synapses was higher at P9–P10, while CI synapses were more prevalent at later developmental stages.

synapses, 0.27 ± 0.03, n = 9, $p > 0.05$; Figure 5F). Taken together, these results indicate that the slower MK-801 block rate observed at CP synapses results from a lower open probability of postsynaptic NMDARs.

Functional Consequences of Differential NMDA Receptor Distribution

Synaptic NMDARs Endow Interneurons with Distinct Firing Properties

The above experiments highlight fundamental differences in NMDAR properties at CI-and CP-mossy fiber-interneuron synapses recorded under voltage-clamp conditions, suggesting potentially different roles for NMDARs at these two synapse types. We next determined the contribution of NMDAR to synaptic activity evoked by single stimuli under current-clamp conditions. Figure 6A illustrates EPSPs evoked by stimulation of CI (top) or CP (middle) synapses. In the absence of added Mg^{2+}, single subthreshold EPSPs were mediated by the activation of both NMDA and AMPARs at both synapse types (Figure 6A). Subtraction of the AMPA EPSP (recorded in the presence of APV) from the total EPSP allowed inspection of the relative contribution of the NMDA EPSP (Figure 6A). The mean NMDA receptor EPSPs were 3.2 ± 0.3 and 1.9 ± 0.3 mV and contributed 37% ± 3% and 21% ± 4% to the peak EPSP at CI (n = 10) and CP synapses (n = 11), respectively (Figure 6A). Given that NMDAR EPSPs are "large and fast" at CI synapses and "small and slow" at CP synapses, we next estimated the relative contribution of the NMDAR EPSP to the total EPSP time course. At the resting membrane potential, NMDA receptors contributed 65% ± 3% (n = 10) to the total integral at CI synapses but only 38% ± 6% (n = 11) at CP synapses.

The different contributions of NMDARs to the EPSP integral at either synapse type suggests that NMDAR EPSPs may differentially influence current summation in response to trains of synaptic stimuli. Indeed, algebraic summation of single EPSPs at a 50 ms interstimulus interval predicts a significantly larger summation of CI-EPSPs than CP-EPSPs (Figures 6B and 6C). To study the contributions of NMDA/AMPAR EPSPs to cellular excitability, EPSP-action potential sequences were evoked by trains of five stimuli at 20 Hz (repeated ten times at 20 s intervals) in the absence or presence of APV under current-clamp conditions. Neurons were then voltage clamped to record AMPA EPSCs. PhTx and DCG-IV were then applied to identify the Ca^{2+}-permeable nature of AMPARs and confirm that the responses were mossy fiber in origin, respectively.

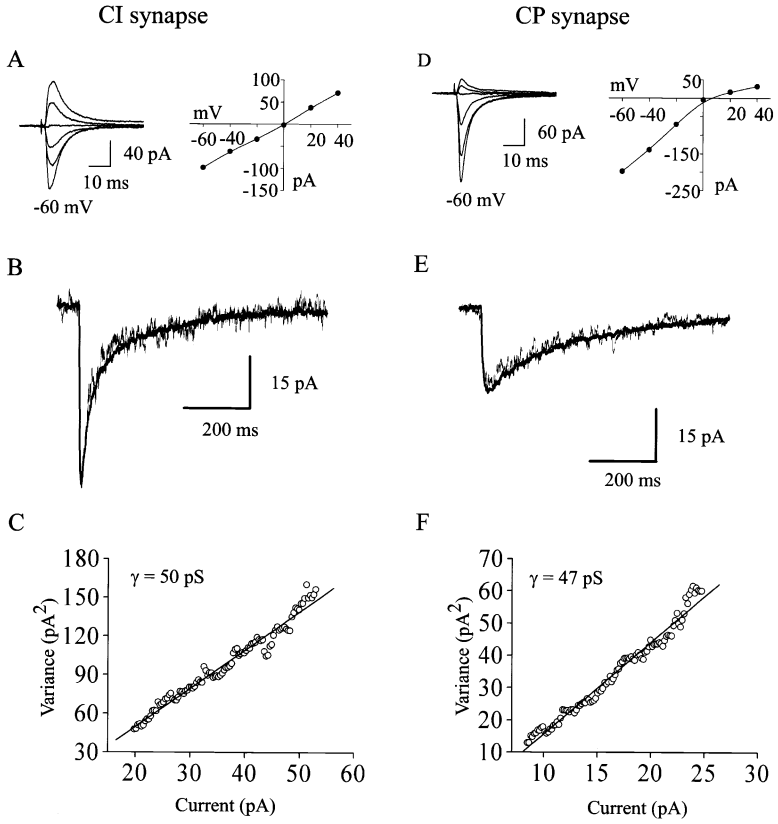

Figure 4. The Single-Channel Conductances of NMDA Receptors at CI and CP Synapses Are Not Significantly Different

(A–C) Data obtained from a CI synapse. (A) The I-V relationship of the AMPA receptor EPSC component from a CI synapse. (B) Method used to compute peak-scaled nonstationary variance of NMDAR-mediated EPSCs. The isolated NMDA EPSC component, averaged from 60 EPSC (dark line) scaled to the peak of a single EPSC (light line). (C) The composite current-variance plot obtained from the analysis of 60 NMDAR EPSCs at CI synapses. Linear relationship of current-variance plot suggests that the open probabilities of NMDARs are low.

(D–F) Identical experiment as that shown in (A)–(C) for NMDAR-mediated EPSCs at CP synapses.

Trains of stimuli elicited EPSPs that summated supralinearly to induce action potential discharge at both synapse types (Figures 6B and 6C). In general, at CI synapses, each stimulus in the train elicited doublets or triplets of action potentials with events later in the train usually resulting in a large depolarizing envelope, presumably reflecting activation of intrinsic conductances on which rode several action potentials (Figure 6B). In contrast, at CP synapses, each stimulus usually elicited only single or doublet action potential firing with little evidence for the late depolarizing phase observed following CI synapse activation (Figure 6C).

In both cases, the number of spikes elicited by the stimulus train was reduced after washing in APV, suggesting that NMDARs contribute significantly to action potential generation at both types of synapse (Figures 6B–6D). The reduction of spike number by APV was most significant at CI synapses and only single action potentials were initiated by each AMPA EPSP, consistent with the large contribution of NMDAR to the total EPSP waveform (Figure 6A).

To quantify these observations, the total number of spikes elicited by the ten trains of stimulation in the absence and presence of APV were estimated. The APV-sensitive and APV-resistant spikes were considered to be generated by NMDA or AMPA receptors, respectively. At CI synapses, the percentage of spikes generated by NMDAR EPSPs was significantly greater (67.6% $\pm$ 4.4%, n = 10) than that observed at CP synapses (40.7% $\pm$ 2.1%, n = 11, $p < 0.01$) (Figure 6D). Taken together, these data indicate that NMDA and AMPA receptors contribute differently to interneuron EPSP-action potential excitability.

NMDAR- and AMPAR-Dependent iLTD

Previous results have suggested that interneuron LTD (iLTD) (McMahon and Kauer, 1997) is not dependent on NMDAR activity, but relies on the influx of postsynaptic Ca^{2+}, possibly via Ca^{2+}-permeable AMPARs, and has previously only been detected at CP synapses (Laezza et al., 1999; Toth et al., 2000). Moreover, we have previously demonstrated that paradigms that induce LTP at mossy fiber-pyramidal neuron synapses induce iLTD at interneuron CP synapses with no evidence for plasticity at CI synapses (Toth et al., 2000). However, all of these previous experiments were performed in the presence of the NMDAR antagonist APV (Toth et al., 2000), and the role of NMDA receptors in mossy fiber-interneuron synaptic plasticity is unknown.

In the final set of experiments, we examined the expression of synaptic plasticity at both synapse types in the presence and absence of APV. Consistent with previous results (Laezza et al., 1999; Toth et al., 2000), in the presence of NMDA receptor antagonists, LTD was observed only at CP synapses in response to 100 Hz stimuli (1 s duration, repeated three times at 10 s intervals) (Figures 7A and 7B). In contrast, in the absence of APV, LTD was observed at both CI and CP synapses (Figures 7C and 7D). At CP synapses, the magnitude of iLTD was similar in the presence or absence of APV (25 min after the induction of LTD, 58.2% $\pm$ 2.9%, n = 7 with APV; 43.9% $\pm$ 3.5%, n = 6 without APV, $p > 0.05$), suggesting little further contribution of NMDARs to iLTD at these synapses. At mossy fiber-pyramidal neuron synapses (another form of CI synapse) long-lasting plasticity is generally considered to be NMDAR independent, although the exact mechanism of induction is somewhat

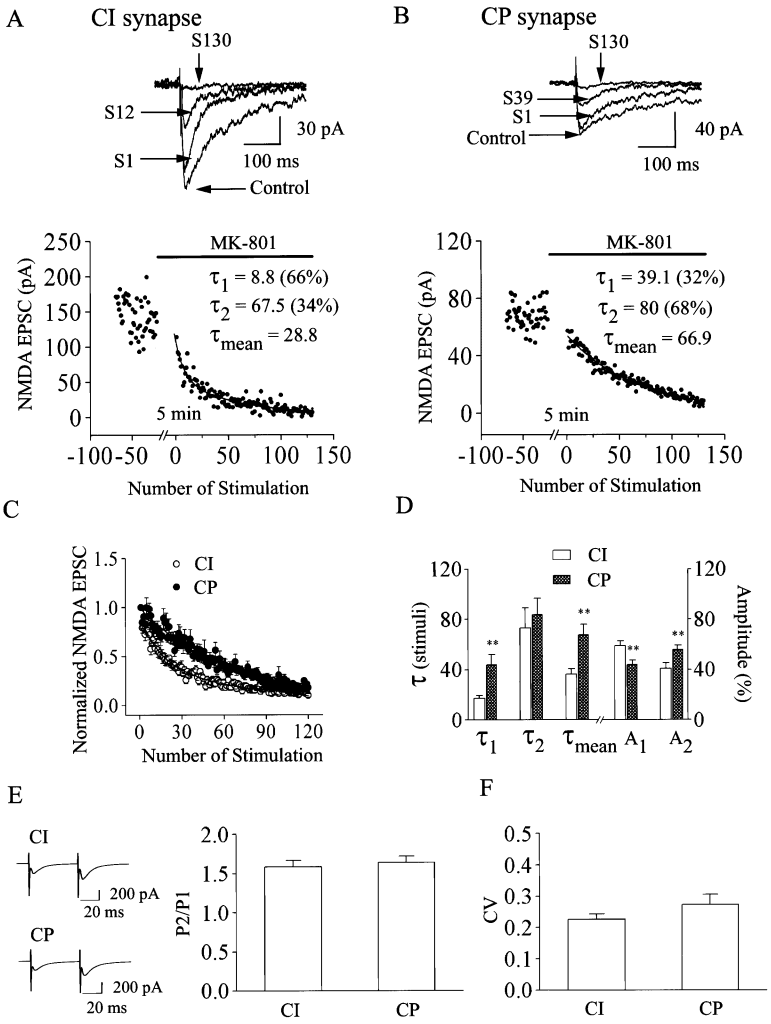

Figure 5. NMDA Receptors at CP Synapses Have Lower Open Probabilities

(A) Time course of block of the isolated NMDA receptor EPSC by MK-801 at a CI synapse (RI = 1.16). After recording basal NMDA EPSCs for 5–10 min, stimulation was stopped, and the slice was perfused with extracellular solution containing MK-801 (40 μM) for 5 min to saturate the synapse with MK-801 before resuming stimulation. Stimulation was then resumed, and the time course of the inhibition of NMDA EPSC was rigorously recorded to evaluate the open probability of NMDA receptors. Upper panel shows current traces evoked by the last basal stimulation before application of MK-801 ("control"), the 1st (S1), 12th (S12), and 130th (S130) stimulation in the presence of MK-801. The relationship of MK-801 inhibition versus the number of stimulation was best fit by a double-exponential function.

(B) Time course of MK-801 block of NMDARs at a CP synapse (RI = 0.17). Experiment was performed in the same way as in (A). MK-801 block rate was slower at this synapse.

(C) Pooled data from nine CP and nine CI synapses illustrates the slower rate of MK-801 block of NMDAR at CP synapses.

(D) Summarized data from nine CP and nine CI synapses. **, $p < 0.01$.

(E) Left panel, current traces from a CI and a CP synapse evoked by a paired-pulse stimulation protocol (interval = 50 ms). Right panel, pooled data for the paired-pulse ratio (PPR) from nine CI and nine CP synapses shown in (C).

(F) Coefficient of variation (CV) of AMPA EPSCs recorded at the same synapses as in (C) and (E). Neither PPR nor CV was significantly different between CI and CP synapses.

controversial (Yeckel et al., 1999; Mellor and Nicoll, 2001). To determine whether iLTD observed at either synapse required postsynaptic elevation of intracellular Ca^{2+}; 20 mM BAPTA was included in the recording electrode (Yeckel et al., 1999). Inclusion of BAPTA in the recording pipette blocked the expression of iLTD at both synapse types, suggesting a role for postsynaptic calcium elevation in induction of both forms of iLTD (Figures 7E and 7F). These results clearly demonstrate that NMDARs at CI synapses participate in the induction of iLTD, whereas at CP synapses, Ca^{2+}-permeable AMPA receptors are sufficient to induce LTD.

Discussion

Dentate granule cells innervate their postsynaptic targets via anatomically specialized synapses. While single granule cells form large, complex "mossy" synapses onto principal neuron targets, GABAergic interneurons are selectively targeted by thin filopodial extensions of mossy terminals and by small en passant boutons (Acsady et al., 1998). The number of filopodial extensions and small terminals is ~10-fold larger than the number of mossy terminals and has led to the suggestion that activity within the mossy fiber pathway engages significantly larger numbers of inhibitory cells than principal cells. This massive recruitment of inhibition has helped explain the physiological observation that increased activity of the granule cells suppresses the overall excitability of the CA3 recurrent system (Bragin et al., 1995a, 1995b; Penttonen et al., 1997), presumably by the monosynaptic recruitment of an extensive network of feedforward inhibitory interneurons (Pouille and Scanziani, 2001).

Our original observations suggested that this anatomical specialization gave rise to a functional segregation of activity that depended on the nature of the postsynaptic target (Maccaferri et al., 1998; Toth and McBain, 1998). Toth et al. (2000) demonstrated a further division of labor within mossy fiber-interneuron projections that was largely based on the presence or absence of GluR2-containing AMPA receptors giving rise to CI- and CP-AMPA synapses respectively. Here we have extended these initial observations and now demonstrate the existence of a continuum of mossy fiber projections to inhibitory interneurons whose properties depend on the nature of *both* AMPA and NMDA receptors expressed at the particular synapse type.

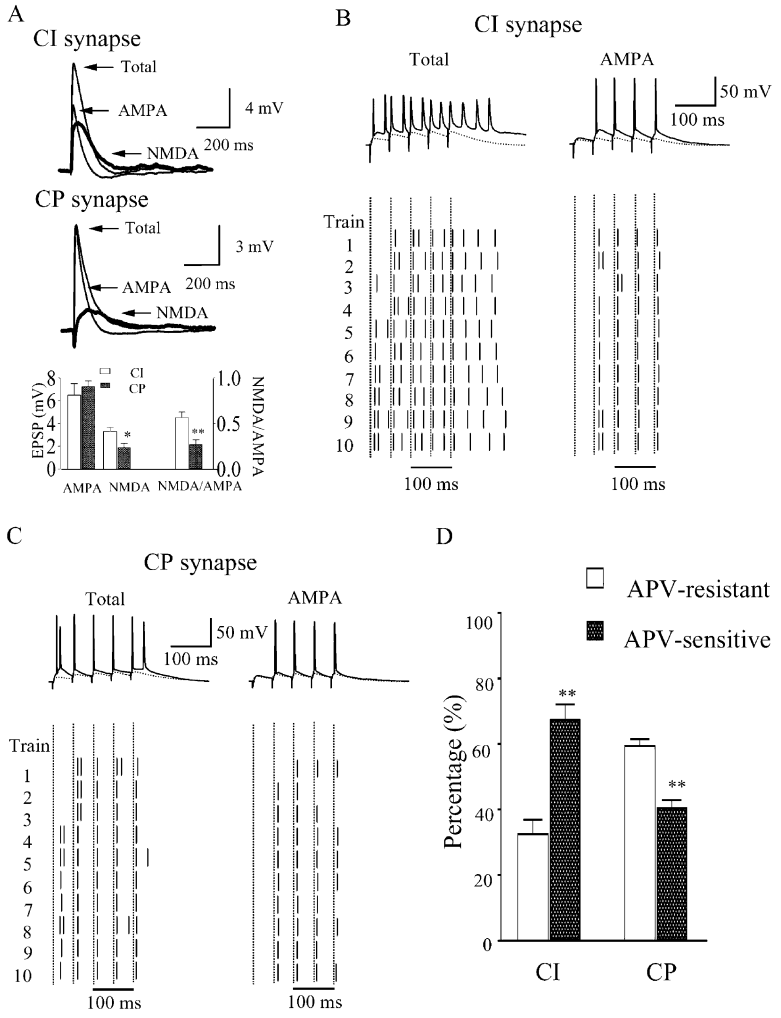

Figure 6. Differential Contributions of NMDARs and AMPARs to Transmission at CI and CP Synapses

(A) Averaged EPSPs recorded in the absence of APV (Total), in the presence of APV (AMPA) and the subtracted, isolated NMDAR-mediated component (NMDA) at a CI (upper panel) and CP synapses (middle panel). Mean data from EPSPs pooled from 11 CP and 10 CI synapses show that the NMDA EPSP and the ratio of NMDA and AMPA EPSPs are significantly lower at CP synapses (lower panel).

(B and C) EPSP/action potential sequences at a CI (B) and a CP synapse (C) elicited by trains of stimuli (five stimuli, 20 Hz, repeat ten times at 20 s intervals) in the absence (left column) or presence (right column) of APV. Upper trace shows a single representative example of an EPSP/action potential sequence elicited by the stimulus train. In this experiment, action potential amplitude was also increased following block of NMDA receptors, suggesting that the depolarizing synaptic envelope leads to a partial inactivation of sodium channels. Dashed waveforms in each of the upper traces is the algebraic summation of five EPSP wavefoms spaced by the interstimulus interval to generate the predicted EPSP summation in the absence of additional intrinsic conductances. Lower panel shows the raster plot of spikes induced by each of the five stimuli in the ten trials. Each short vertical line represents a single action potential whose position in the raster plot represents the actual timing of the action potential waveform. Dashed lines represent the timing of the stimulus artifact.

(D) Differential contribution of NMDA (APV-sensitive) and AMPA (APV-resistant) receptors to cellular excitability at CI and CP synapses. **, $p < 0.01$. Note that NMDARs make the major contribution to the number of action potentials elicited in response to activation of CI synapses. In contrast, NMDAR make only a modest contribution to action potential generation following CP synapse activation.

The subunit composition and kinetic properties of NMDARs allow them to play differential roles at CI and CP synapses. NMDARs at CI synapses play a major role in synaptic transmission and are involved in the induction of a novel form of iLTD, whereas only a modest role for NMDARs was observed at CP synapses, and long-term plasticity was NMDAR independent. NMDARs at CP synapses possess a higher proportion of NR2B subunits and have a lower open probability than NMDARs at CI synapses; contributing to the smaller amplitude and slower kinetics of NMDAR EPSCs at CP synapses, although differences in channel density cannot be ruled out.

It is important to point out that for ease of discussion, we have concentrated on CI and CP synapses, which represent the extreme ends of a continuum of synaptic types, and mossy fiber-interneuron synapses also comprise a "mixed" phenotype based on AMPAR sensitivity to PhTx, rectification index, or NMDAR properties. Whether this reflects a pool of synapses undergoing developmental regulation or activity-dependent conversion of one synapse type into another, remains unclear. We also considered the possibility that the mixed synapse type represented experiments where we were stimulating multiple fibers activating overlapping CI and CP synapse populations; in fact, in our previous investigations (Toth and McBain, 1998; Toth et al., 2000), synapses with this phenotype were omitted from the analysis based on this reasoning. We now consider this to be highly unlikely. Experiments involving rigorous quantal analysis of single mossy fiber-evoked EPSCs have a similar range of PhTx block (J.J.L. and C.M., unpublished data), indicating that this population represents a legitimate mossy fiber-interneuron class. Experiments investigating the effects of philanthotoxin block on miniature synaptic events may allow a further test of this hypothesis. However, it is worthwhile noting that in addition to receiving mossy fiber inputs, stratum lucidum interneurons also receive synaptic input from CA3 pyramidal neurons potentially complicating the separation and identification of each miniature population.

In a number of systems, the subunit compositions of both NMDARs and AMPARs are developmentally regulated. Typically, NR2B subunits are abundant at early

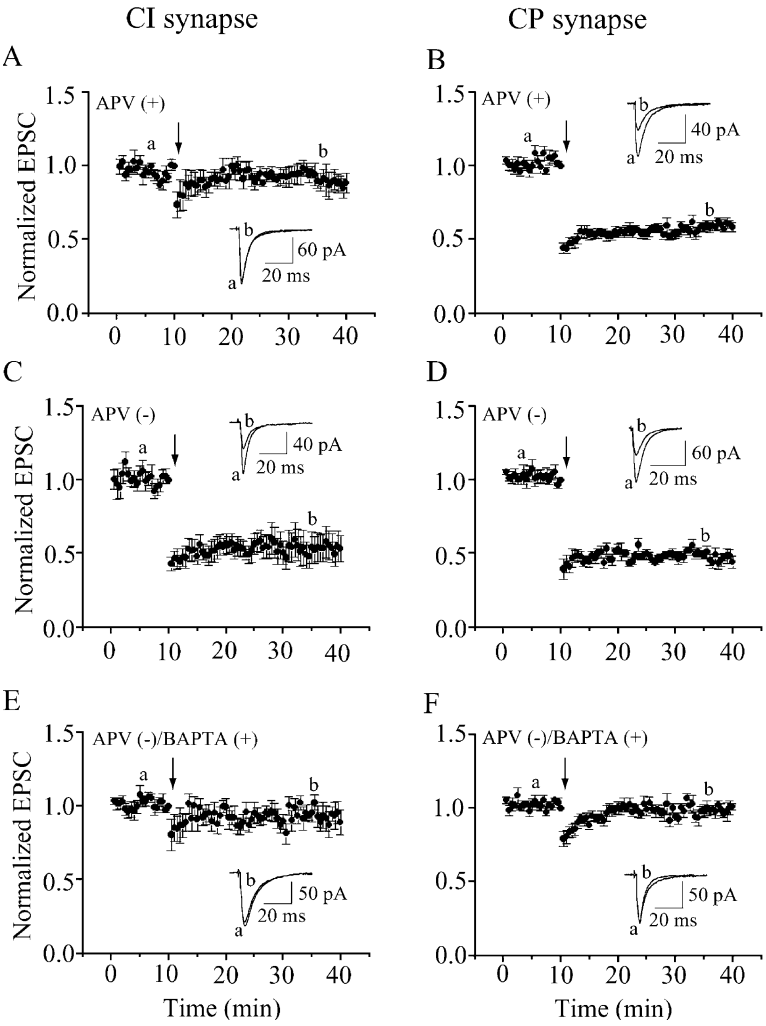

Figure 7. Differential Forms of iLTD Exist at Mossy Fiber-Interneuron Synapses

(A) High-frequency stimulation (100 Hz, 1 s duration, repeated three times at 10 s intervals) failed to induce iLTD at CI synapses in the presence of 100 μM APV (n = 6).

(B) The same stimulation protocol as in (A) induced iLTD at CP synapses in the presence of 100 μM APV (n = 7).

(C and D) In the absence of APV, the induction protocol induced iLTD at both CI (n = 5, [C]) and CP synapses (n = 6, [D]).

(E and F) Inclusion of 20 mM BAPTA in the recording pipette prevented LTD at both CI (n = 6, [E]) and CP synapses (n = 7, [F]).

developmental stages and are progressively replaced by NR2A during development (Monyer et al., 1994; Flint et al., 1997; Stocca and Vicini, 1998; Cathala et al., 2000). In *Xenopus* spinal interneurons, Ca^{2+}-permeable AMPARs mediate synaptic transmission at early embryonic stages and are replaced by Ca^{2+}-impermeable AMPARs on maturation (Rohrbough and Spitzer, 1999). In cultured hippocampal neurons or hippocampal slices, GluR2 expression increases with the increase of culture time (Pickard et al., 2000) or animal age (Zhu et al., 2000). Such observations have led to the general assumption that synapses at earlier stages of development contain NMDARs with higher levels of NR2B, and AMPARs with lower levels of GluR2. Our results are suggestive of such developmental regulation and indicate that CP synapses containing Ca^{2+}-permeable AMPARs (little or no GluR2) and NMDARs with a higher level of NR2B composition predominate at earlier developmental ages. However, it is important to point out that significant numbers of both synapse type were observed at the latest development stage (>P30), suggesting that while developmental regulation of synapse phenotype may exist, both extreme ends of the continuum exist in parallel at mature stages.

While NMDA and AMPARs are generally considered to be colocalized postsynaptically at many mature central glutamatergic synapses and are activated by presynaptically released glutamate, the development or maturation of NMDA and AMPARs is not necessarily synchronized. NMDARs are detected first at developing excitatory synapses in mammalian hippocampus (Durand et al., 1996; Liao et al., 1999). Functional AMPAR expression can be induced at initially silent synapses by NMDAR activation (Liao et al., 1995; Isaac et al., 1995; Durand et al., 1996), suggesting that NMDAR activation is required for subsequent AMPAR expression at developing glutamatergic synapses. Moreover, NMDA and especially AMPARs undergo membrane trafficking (Haas, 2001). Thus, an alternative explanation for the distinct expression of NMDA and AMPARs at CI and CP synapses may be that NMDA and AMPARs at either synapse are mutually regulated. It is possible that intracellular signaling pathways activated by Ca^{2+}-permeable AMPARs may selectively attract or expel NMDAR subunits such as NR2B or NR2A to or from the postsynaptic density. Conversely, the function of NMDARs located at this domain may also act to regulate the expression of GluR2 or other AMPA receptor subunits. Experiments are currently underway to determine the interplay between NMDA and AMPA receptor subunit distributions at these synapses.

Roles of NMDA and AMPARs in Synaptic Transmission and Plasticity at CI and CP Synapses

The different composition and function of NMDA and AMPA receptors expressed at CI and CP synapses was strongly correlated with their distinct roles in synaptic transmission at these two synapse types. Repetitive activation of CI synapses elicited progressively more action potentials per stimulus during a train than at CP synapses, presumably due to the temporal summation of their larger amplitude NMDAR EPSCs. During trains of stimuli, multiple action potentials were evoked by each stimulus, while those occurring later in the train consistently evoked a large, long-lasting depolarization that resulted in the generation of numerous action potentials long after the train had ceased. Such a mechanism will ensure significant temporal summation of synaptic events, triggering a robust doublet or triplet action potential discharge in response to activation of CI synapses. Block of NMDARs at these synapses removed this phenomenon, underscoring the important role for NMDA receptors at these synapses. In contrast, the contribution of NMDARs to cellular excitability was more modest at CP synapses.

Fricker and Miles (2000) have recently shown that EPSPs initiate action potential firing with short latencies and precise timing in most CA1 hippocampal inhibitory neurons, but result in delayed and variable firing patterns in pyramidal neurons. Their data suggest that action potential firing depends on the delicate balance of subthreshold intrinsic currents; EPSPs activate outward potassium currents which prevent the generation of delayed spikes in interneurons, but favor inward sodium currents which produce plateau potentials leading to the observed long latency action potentials in pyramidal cells (Fricker and Miles, 2000). In our experiments, the differential firing patterns and the prolonged firing after the termination of stimulus trains at CI synapses (Figure 6B) suggests that EPSPs at these synapses may activate repertoires of intrinsic currents in interneurons distinct from those activated by CP synapses. The degree of intrinsic current activation presumably is strongly influenced by the shape of the EPSP waveform, the release properties of each individual synapse type, and/or the electrotonic location of the synaptic input site.

NMDARs at CI synapses were also intimately involved in the induction of a previously undescribed form of iLTD (McMahon and Kauer, 1997, Laezza et al., 1999, Toth et al., 2000). In contrast, iLTD at CP synapses was NMDAR independent, consistent with previous reports (Toth et al., 2000). Our previous studies (Maccaferri et al., 1998, Toth et al., 2000) indicated a lack of plasticity at CI synapses in response to paradigms that induced LTP at mossy fiber-principal cells synapses and iLTD at interneuron-CP synapses. However, these previous studies were performed in the presence of NMDA receptor antagonists. The present results demonstrate that mossy fiber-interneuron synapses possess diverse forms of plasticity. Both forms of iLTD required elevation of postsynaptic Ca^{2+} because induction was prevented by inclusion of BAPTA in the recording pipette (Yeckel et al., 1999). The existence of two forms of iLTD that can be induced by similar stimulus paradigms that induce LTP at mossy fiber-principal neuron synapses suggests that mechanisms that differentially regulate Ca^{2+}-permeable AMPA receptors and NMDA receptors (e.g., phosphorylation or receptor trafficking) may independently influence the dynamic state of synaptic efficacy at CI and CP synapses.

In conclusion, we have demonstrated that the mossy fiber-CA3 inhibitory interneuron system consists of a continuum of synapse types that may expand the repertoire of activity engaged by granule cell activity within the CA3 network.

Experimental Procedures

Hippocampal Slice Preparation

Transverse hippocampal slices (300 μm) were obtained from Sprague Dawley rats as described previously (Toth and McBain, 1998). The ages of the rats were typically 16–20 days unless stated otherwise in the text. Rats were deeply anesthetized with isoflurane, and the brain dissected out in ice-cold saline solution containing 130 mM NaCl, 24 mM $NaHCO_3$, 3.5 mM KCl, 1.25 mM NaH_2PO_4, 1.0 mM $CaCl_2$, 5.0 mM $MgCl_2$, and 10 mM glucose, saturated with 95% O_2/5% CO_2, pH 7.4. All animal procedures conformed to the National Institutes of Health animal welfare guidelines.

Voltage-Clamp Recordings

Whole-cell patch-clamp recordings were made from visually identified interneurons located within the stratum lucidum of CA3 by the use of a modified Axopatch 200A amplifier (Axon Instruments, Foster City, CA) in voltage-clamp mode. Unless stated otherwise, recording electrodes were filled with 100 mM Cs-gluconate, 0.6 mM EGTA, 5 mM $MgCl_2$, 8 mM NaCl, 2 mM ATP_2Na, 0.3 mM GTPNa, 40 mM HEPES, 0.1 mM spermine, and 1 mM QX-314, pH 7.2–7.3. Biocytin (0.2%) was added to the recording electrode solution to allow post hoc morphological processing of every recorded cell (Toth and McBain, 1998). The extracellular solution comprised the following composition: 130 mM NaCl, 24 mM $NaHCO_3$, 3.5 mM KCl, 1.25 mM $NaHPO_4$, 2.5 mM $CaCl_2$, and 10 mM glucose, saturated with 95% O_2 and 5% CO_2, pH 7.4. Bicuculline methobromide (100 μM) and glycine (10 μM) were routinely added and Mg^{2+} omitted from the above solution to inhibit GABA receptor-mediated IPSCs and facilitate the recording of NMDAR EPSCs, respectively. Under these conditions, dual component EPSCs mediated by both AMPA and NMDARs were recorded. AMPAR-mediated EPSCs were isolated by including Mg^{2+} (1.5 mM) and *dl*-APV (100 μM) in the extracellular solution. NMDA EPSCs were obtained either by digital subtraction of the AMPA component (recorded in the presence of Mg^{2+} and APV) from the dual component EPSC recorded in the absence of Mg^{2+} and APV or by including DNQX (10 μM) in the extracellular solution (see Results). In all experiments, the Group II mGluR agonist DCG-IV (1 μM) was added to the perfusate to confirm that synaptic events were mossy fiber in origin (Kamiya et al., 1996; Toth and McBain, 1998; Toth et al., 2000).

All cells were initially identified on the basis of somata shape and position within the CA3 stratum lucidum subfield using infrared video microscopy and differential interference contrast optics. Confirmation that cells were inhibitory interneurons was made using post hoc biocytin processing. Recordings were made at room temperature (~24°C) at a holding potential of −60 mV, unless otherwise indicated. Series resistance was rigorously monitored by the delivery of a 5 mV voltage step after each evoked EPSC. Experiments were discontinued if the series resistance changed by >10%. Synaptic responses were evoked by low-intensity stimulation (80 μs duration; 40–80 μA intensity) of granule cells in the dentate gyrus or the stratum lucidum of the hippocampal CA3 region via a constant-current isolation unit (A360; World Precision Instrument, Sarasota, FL) connected to a patch electrode that was filled with oxygenated extracellular solution. For a single neuron, the stimulus intensity was set to the lowest value that reliably evoked a single EPSC waveform without obvious failure. Synaptic responses were included in the analysis if the rise times and decay time constants were monotonic and possessed no apparent multiple EPSCs or polysynaptic waveforms. At the end of each experiment, a solution containing APV,

bicuculine, and DNQX was perfused to record the isolated stimulus artifact, which was then averaged and subtracted from synaptic records to obtain stimulus artifact-free records of EPSCs for accurate amplitude measurement.

Interneuron LTD (iLTD) was induced by a high-frequency induction protocol comprising a 100 Hz train of stimuli, 1 s in duration, repeated three times at 10 s intervals (Maccaferri et al., 1998; Toth et al., 2000). The extracellular solution contained 1.5 mM Mg^{2+} with or without *dl*-APV (100 μM). For some experiments, the intracellular EGTA was replaced with 20 mM BAPTA as stated in the text.

Current-Clamp Recordings

Whole-cell recordings were initially obtained in voltage-clamp mode and then switched to current clamp to record EPSPs and action potentials. For this series of experiments, Cs-gluconate in the intracellular solution was replaced with the same concentration of K-gluconate, and QX-314 was omitted. After recording EPSPs with a single stimulus protocol (0.33 Hz), a multiple stimulus protocol (five stimuli at 20 Hz, repeated ten times at an interval of 20 s) was used to study the summation of EPSPs and action potential induction for each cell. During current clamp, cells were kept at their resting membrane potential (normally between −60 and −70 mV) and were discarded if not stable throughout the experiment. Data from those cells whose resting membrane potentials were less than −60 mV or varied more than 10 mV during the experiments were excluded from analysis.

Peak-Scaled Nonstationary Variance Analysis

Peak-scaled nonstationary variance analysis was used to estimate the conductance of synaptic NMDARs (Robinson et al., 1991; Traynelis et al., 1993; Traynelis and Jaramillo, 1998; Benke et al., 1998). The recorded NMDA EPSCs were initially inspected visually to exclude those responses contaminated with spontaneous synaptic activity. Only those traces showing fast rise time and smooth decay were selected for analysis. The selected EPSCs (50–100) were aligned and averaged. The average response was scaled to the peak and subtracted from individual responses to compute the variance. EPSC responses 400 ms from the peak event were selected for analysis to ensure measurement of the NMDA receptor-mediated component. The average EPSC response was then divided into 100 equally sized bins and the corresponding variances pooled. The binned variance was plotted against the mean current amplitude, and the single-channel current was estimated by fitting the data according to either of the following equations: (1) $\sigma^2 = iI - I^2/N + \sigma_{base}$, when the open probability was high; or (2) $\sigma^2 = iI + \sigma_{base}$, when the open probability was low (Robinson et al., 1991; Traynelis and Jaramillo, 1998), where σ^2 is the variance, I is the mean current, N is the number of channels activated at the peak of the mean current, i is the single-channel current, and σ_{base} is the background variance. Since NMDARs at central synapses usually possess low open probabilities (Rosenmund et al., 1995), most of our data was fitted by Equation 2, which is a linear function. This is consistent with previous results, which also showed a linear variance and current relationship for NMDA EPSC (Robinson et al., 1991). The single-channel conductance was measured by $\gamma = i/(E - E_{rev})$, where E is the holding potential, and E_{rev} is the reversal potential (obtained by extrapolating linear fitting of the I-V curve at the negative potentials to $I = 0$).

Data Analysis

Current traces displayed in the figures are averages of more than 20 AMPA EPSCs or more than 50 NMDA EPSCs. NMDA EPSC decay time constants were obtained by fitting the averaged NMDA EPSCs normally with two-exponential functions. Weighted time constants were computed by equation: $\tau = \tau_1 \times A_1/(A_1 + A_2) + \tau_2 \times A_2/(A_1 + A_2)$, where τ_1 and τ_2 were the two fitted time constants, and A_1 and A_2 were their corresponding amplitudes. Time course of MK-801 block was fitted by double-exponential functions. Data are presented as means ± SEM. Unpaired or paired Student's t tests were used for statistical analysis as appropriate; p values are reported throughout the text.

The rectification index (RI) of AMPA EPSCs was generated from averaged (20–30 traces) AMPA EPSC amplitudes at different holding potentials. Data recorded at the negative holding potentials (from −60 to −20 mV) were fit by a linear regression. The RI of the I-V relationship was then defined as the ratio of the actual current amplitude at +40 mV to the predicted linear value at +40 mV (extrapolated from linear fitting of the currents at the negative potentials; Liu and Cull-Candy [2000]). A high RI value means that the I-V curve is more linear, and the AMPA receptors have a low Ca^{2+} permeability and vice versa.

Chemicals

All compounds were obtained from Sigma-Aldrich (St. Louis, MO) unless stated otherwise. Philanthotoxin-433 tris-trifluoracetate (PhTx) was obtained from Research Biochemicals (Natick, MA). (2S,2′R,3′R)-2-(2′,3′-dicarboxycyclopropyl)glycine (DCG-IV) was obtained from Tocris Cookson (Ballwin, MO).

Acknowledgments

The authors would like to thank Dr. Josh Lawrence and Mr. Harrison Walker for critically reading the manuscript and the Labs of Jeff Diamond and Dietmar Plenz for helpful discussion throughout the course of this study. We would like to thank Emily Philips-Tansey and Orinthial MacIntire for performing all post hoc morphology. C.M. was supported by the NICHD Intramural Research Program and the Human Frontier Science Program.

Received: October 22, 2001
Revised: January 11, 2002

References

Acsady, L., Kamondi, A., Sik, A., Freund, T., and Buzsaki, G. (1998). GABAergic cells are the major postsynaptic targets of mossy fibers in the rat hippocampus. J. Neurosci. *18*, 3386–3403.

Amaral, D.G., and Dent, J.A. (1981). Development of the mossy fibers of the dentate gyrus. I. A light and electron microscopic study of the mossy fibers and their expansions. J. Comp. Neurol. *195*, 51–86.

Benke, T.A., Luthi, A., Isaac, J.T., and Collingridge, G.L. (1998). Modulation of AMPA receptor unitary conductance by synaptic activity. Nature *393*, 793–797.

Blaschke, M., Keller, B.U., Rivosecchi, R., Hollmann, M., Heinemann, S., and Konnerth, A. (1993). A single amino acid determines the subunit-specific spider toxin block of alpha-amino-3-hydroxy-5-methylisoxazole-4-propionate/kainate receptor channels. Proc. Natl. Acad. Sci. USA *90*, 6528–6532.

Bowie, D., and Mayer, M.L. (1995). Inward rectification of both AMPA and kainate subtype glutamate receptors generated by polyamine-mediated ion channel block. Neuron *15*, 453–462.

Bragin, A., Jando, G., Nadasdy, Z., Hetke, J., Wise, K., and Buzsaki, G. (1995a). Gamma (40–100 Hz) oscillation in the hippocampus of the behaving rat. J. Neurosci. *15*, 47–60.

Bragin, A., Jando, G., Nadasdy, Z., van Landeghem, M., and Buzsaki, G. (1995b). Dentate EEG spikes and associated interneuronal population bursts in the hippocampal hilar region of the rat. J. Neurophysiol. *73*, 1691–1705.

Cathala, L., Misra, C., and Cull-Candy, S. (2000). Developmental profile of the changing properties of NMDA receptors at cerebellar mossy fiber-granule cell synapses. J. Neurosci. *20*, 5899–5905.

Chattarji, S., Stanton, P.K., and Sejnowski, T.J. (1989). Commissural synapses, but not mossy fiber synapses, in hippocampal field CA3 exhibit associative long-term potentiation and depression. Brain Res. *495*, 145–150.

Dingledine, R., Borges, K., Bowie, D., and Traynelis, S.F. (1999). The glutamate receptor ion channels. Pharmacol. Rev. *51*, 7–61.

Donevan, S.D., and Rogawski, M.A. (1995). Intracellular polyamines mediate inward rectification of Ca^{2+}-permeable α-amino-3-hydroxy-5-methyl-4-isoxazolepropionic acid receptors. Proc. Natl. Acad. Sci. USA *92*, 9298–9302.

Durand, G.M., Kovalchuk, Y., and Konnerth, A. (1996). Long-term potentiation and functional synapse induction in developing hippocampus. Nature *381*, 71–75.

Flint, A.C., Maisch, U.S., Weishaupt, J.H., Kriegstein, A.R., and Mon-

yer, H. (1997). NR2A subunit expression shortens NMDA receptor synaptic currents in developing neocortex. J. Neurosci. *17*, 2469–2476.

Fricker, D., and Miles, R. (2000). EPSP amplification and the precision of spike timing in hippocampal neurons. Neuron *28*, 559–569.

Haas, K. (2001). Directing AMPA receptor traffic. Trends Neurosci. *24*, 137.

He, Y., Janssen, W.G., Vissavajjhala, P., and Morrison, J.H. (1998). Synaptic distribution of GluR2 in hippocampal GABAergic interneurons and pyramidal cells: a double-label immunogold analysis. Exp. Neurol. *150*, 1–13.

Herlitze, S., Raditsch, M., Ruppersberg, J.P., Jahn, W., Monyer, H., Schoepfer, R., and Witzemann, V. (1993). Argiotoxin detects molecular differences in AMPA receptor channels. Neuron *10*, 1131–1140.

Hessler, N.A., Shirke, A.M., and Malinow, R. (1993). The probability of transmitter release at a mammalian central synapse. Nature *66*, 569–572.

Huettner, J.E., and Bean, B.P. (1988). Block of N-methyl-D-aspartate-activated current by the anticonvulsant MK-801: selective binding to open channels. Proc. Natl. Acad. Sci. USA *85*, 1307–1311.

Isaac, J.T., Nicoll, R.A., and Malenka, R.C. (1995). Evidence for silent synapses: implications for the expression of LTP. Neuron *15*, 427–434.

Jahr, C.E. (1992). High probability opening of NMDA receptor channels by L-glutamate. Science *255*, 470–472.

Jonas, P., Major, G., and Sakmann, B. (1993). Quantal components of unitary EPSCs at the mossy fibre synapse on CA3 pyramidal cells of rat hippocampus. J. Physiol. *472*, 615–663.

Kamboj, S.K., Swanson, G.T., and Cull-Candy, S.G. (1995). Intracellular spermine confers rectification on rat calcium-permeable AMPA and kainate receptors. J. Physiol. *486*, 297–303.

Kamiya, H., Shinozaki, H., and Yamamoto, C. (1996). Activation of metabotropic glutamate receptor type 2/3 suppresses transmission at rat hippocampal mossy fibre synapses. J. Physiol. *493*, 447–455.

Koh, D.S., Burnashev, N., and Jonas, P. (1995). Block of native Ca^{2+}-permeable AMPA receptors in rat brain by intracellular polyamines generates double rectification. J. Physiol. *486*, 305–312.

Laezza, F., Doherty, J.J., and Dingledine, R. (1999). Long-term depression in hippocampal interneurons: joint requirement for pre- and postsynaptic events. Science *285*, 1411–1414.

Langdon, R.B., Johnson, J.W., and Barrionuevo, G. (1995). Post-tetanic potentiation and presynaptically induced long-term potentiation at the mossy fiber synapse in rat hippocampus. J. Neurobiol. *26*, 370–385.

Leranth, C., Szeidemann, Z., Hsu, M., and Buzsaki, G. (1996). AMPA receptors in the rat and primate hippocampus: a possible absence of GluR2/3 subunits in most interneurons. Neuroscience *70*, 631–652.

Liao, D., Hessler, N.A., and Malinow, R. (1995). Activation of postsynaptically silent synapses during pairing-induced LTP in CA1 region of hippocampal slice. Nature *375*, 400–404.

Liao, D., Zhang, X., O'Brien, R., Ehlers, M.D., and Huganir, R.L. (1999). Regulation of morphological postsynaptic silent synapses in developing hippocampal neurons. Nat. Neurosci. *2*, 37–43.

Liu, S.Q., and Cull-Candy, S.G. (2000). Synaptic activity at calcium-permeable AMPA receptors induces a switch in receptor subtype. Nature *405*, 454–458.

Maccaferri, G., Toth, K., and McBain, C.J. (1998). Target-specific expression of presynaptic mossy fiber plasticity. Science *279*, 1368–1370.

McBain, C.J., and Fisahn, A. (2001). Interneurons unbound. Nat. Rev. Neurosci. *2*, 11–23.

McBain, C.J., and Mayer, M.L. (1994). N-methyl-D-aspartic acid receptor structure and function. Physiol. Rev. *74*, 723–760.

McMahon, L.L., and Kauer, J.A. (1997). Hippocampal interneurons express a novel form of synaptic plasticity. Neuron *18*, 295–305.

Mellor, J., and Nicoll, R.A. (2001). Hippocampal mossy fiber LTP is independent of postsynaptic calcium. Nat. Neurosci. *4*, 125–126.

Monaghan, D.T., and Cotman, C.W. (1985). Distribution of N-methyl-D-aspartate-sensitive L-[3H]glutamate-binding sites in rat brain. J. Neurosci. *5*, 2909–2919.

Monyer, H., Burnashev, N., Laurie, D.J., Sakmann, B., and Seeburg, P.H. (1994). Developmental and regional expression in the rat brain and functional properties of four NMDA receptors. Neuron *12*, 529–540.

Penttonen, M., Kamondi, A., Sik, A., Acsady, L., and Buzsaki, G. (1997). Feed-forward and feed-back activation of the dentate gyrus in vivo during dentate spikes and sharp wave bursts. Hippocampus *7*, 437–450.

Pickard, L., Noël, J., Henley, J.M., Collingridge, G.L., and Molnar, E. (2000). Developmental changes in synaptic AMPA and NMDA receptor distribution and AMPA receptor subunit composition in living hippocampal neurons. J. Neurosci. *20*, 7922–7931.

Pouille, F., and Scanziani, M. (2001). Enforcement of temporal fidelity in pyramidal cells by somatic feed-forward inhibition. Science *293*, 1159–1163.

Robinson, H.P., Sahara, Y., and Kawai, N. (1991). Nonstationary fluctuation analysis and direct resolution of single channel currents at postsynaptic sites. Biophys. J. *59*, 295–304.

Rohrbough, J., and Spitzer, N.C. (1999). Ca^{2+}-permeable AMPA receptors and spontaneous presynaptic transmitter release at developing excitatory spinal synapses. J. Neurosci. *19*, 8528–8541.

Rosenmund, C., Clements, J.D., and Westbrook, G.L. (1993). Nonuniform probability of glutamate release at a hippocampal synapse. Science *262*, 754–757.

Rosenmund, C., Feltz, A., and Westbrook, G.L. (1995). Synaptic NMDA receptor channels have a low open probability. J. Neurosci. *15*, 2788–2795.

Siegel, S.J., Brose, N., Janssen, W.G., Gasic, G.P., Jahn, R., Heinemann, S.F., and Morrison, J.H. (1994). Regional, cellular, and ultrastructural distribution of N-methyl-D-aspartate receptor subunit 1 in monkey hippocampus. Proc. Natl. Acad. Sci. USA *91*, 564–568.

Spruston, N.P., Jonas, P., and Sakmann, B. (1995). Dendritic glutamate receptor channels in rat hippocampal CA3 and CA1 pyramidal neurons. J. Physiol. *482*, 325–352.

Stocca, G., and Vicini, S. (1998). Increased contribution of NR2A subunit to synaptic NMDA receptors in developing rat cortical neurons. J. Physiol. *507*, 13–24.

Toth, K., and McBain, C.J. (1998). Afferent-specific innervation of two distinct AMPA receptor subtypes on single hippocampal interneurons. Nat. Neurosci. *1*, 572–578.

Toth, K., Suares, G., Lawrence, J.J., Philips-Tansey, E., and McBain, C.J. (2000). Differential mechanisms of transmission at three types of mossy fiber synapse. J. Neurosci. *20*, 8279–8289.

Traynelis, S.F., and Jaramillo, F. (1998). Getting the most out of noise in the central nervous system. Trends Neurosci. *21*, 137–145.

Traynelis, S.F., Silver, R.A., and Cull-Candy, S.G. (1993). Estimated conductance of glutamate receptor channels activated during EPSCs at the cerebellar mossy fiber-granule cell synapse. Neuron *11*, 279–289.

Washburn, M.S., and Dingledine, R. (1996). Block of alpha-amino-3-hydroxy-5-methyl-4-isoxazolepropionic acid (AMPA) receptors by polyamines and polyamine toxins. J. Pharmacol. Exp. Ther. *278*, 669–678.

Watanabe, M., Fukaya, M., Sakimura, K., Manabe, T., Mishina, M., and Inoue, Y. (1998). Selective scarcity of NMDA receptor channel subunits in the stratum lucidum (mossy fibre-recipient layer) of the mouse hippocampal CA3 subfield. Eur. J. Neurosci. *10*, 478–487.

Weisskopf, M.G., and Nicoll, R.A. (1995). Presynaptic changes during mossy fibre LTP revealed by NMDA receptor-mediated synaptic responses. Nature *376*, 256–259.

Williams, K. (1993). Ifenprodil discriminates subtypes of the N-methyl-D-aspartate receptor: selectivity and mechanisms at recombinant heteromeric receptors. Mol. Pharmacol. *44*, 851–859.

Yeckel, M.F., Kapur, A., and Johnston, D. (1999). Multiple forms

of LTP in hippocampal CA3 neurons use a common postsynaptic mechanism. Nat. Neurosci. *2*, 625–633.

Zalutsky, R.A., and Nicoll, R.A. (1992). Mossy fiber long-term potentiation shows specificity but no apparent cooperativity. Neurosci. Lett. *138*, 193–197.

Zhu, J.J., Esteban, J.A., Hayashi, Y., and Malinow, R. (2000). Postnatal synaptic potentiation: delivery of GluR4-containing AMPA receptors by spontaneous activity. Nat. Neurosci. *3*, 1098–1106.